Bioactive Materials 5 (2020) 758–767

Contents lists available at ScienceDirect

Bioactive Materials

journal homepage: http://www.keaipublishing.com/biomat

Gadolinium-hyaluronic acid nanoparticles as an efficient and safe magnetic resonance imaging contrast agent for articular cartilage injury detection

Rong Lu[a], Yuyang Zhang[a], Hongyue Tao[a], Lu Zhou[b], Huidi Li[b], Tianwu Chen[c], Peng Zhang[c], Yao Lu[d,e,*], Shuang Chen[a,**]

[a] Department of Radiology, Huashan Hospital, Fudan University, Shanghai, 200040, China
[b] Department of Medicinal Chemistry, School of Pharmacy, Fudan University, Shanghai, 201203, China
[c] Department of Sports Medicine, Huashan Hospital, Fudan University, Shanghai, 200040, China
[d] Guangdong Key Lab of Orthopedic Technology and Implant Materials, Key Laboratory of Trauma & Tissue Repair of Tropical Area of PLA, Guangzhou, Guangdong, 510010, China
[e] Orthopedic Centre, Clinical Research Centre, Zhujiang Hospital, Southern Medical University, Guangzhou, Guangdong, 510280, China

ARTICLE INFO

Keywords:
Hyaluronic acid
Gadolinium
Nanoparticles
Magnetic resonance imaging contrast agents
Cartilage injury

ABSTRACT

Accurate detection of cartilage injuries is critical for their proper treatment because these injuries lack the self-healing ability and lead to joint dysfunction. However, the low longitudinal T1 relaxivity ($r1$) and non-specificity of contrast agents (such as gadolinium(III)-diethylenetriamine-pentaacetic acid (Gd-DTPA)) significantly limit the efficiency of clinical magnetic resonance imaging (MRI) applications. To overcome these drawbacks, we integrated hyaluronic acid (HA) with Gd to synthesize a Gd-DTPA-HA composite, which was subsequently freeze-dried to produce nanoparticles (NPs). The resultant Gd-HA NPs demonstrated a greater $r1$ value (12.51 mM^{-1} s^{-1}) compared with the bulk Gd-DTPA-HA (8.37 mM^{-1} s^{-1}) and clinically used Gd-DTPA (3.88 mM^{-1} s^{-1}). Moreover, the high affinity of HA to the cartilage allowed these NPs to penetrate deeper beyond the cartilage surface. As a result, Gd-HA NPs considerably increased the quality of cartilage and lesion MR images via their intra-articular injection *in vivo*. Specifically, 2 h after NP administration, the signal-to-noise ratio at the injured cartilage site was 2.3 times greater than the value measured before the injection. In addition, Gd-HA NPs exhibited good biosafety properties due to the absence of adverse effects in the blood or on the main organs. It was also showed that Gd NPs were first metabolized by the kidney and liver and then excreted from the body with urine. Thus, Gd-HA NPs can potentially serve as an efficient MRI contrast agent for improved detection of cartilage injuries.

1. Introduction

Articular cartilage is a highly specialized tissue that contains no blood supplies, nerve tissues, or lymph tissues. Once injured, the cartilage cannot self-heal, resulting in joint degeneration and dysfunction. Thus, accurate assessment of the lesion morphology and degree is especially crucial for the diagnosis, prognosis, and treatment of cartilage injuries. Magnetic resonance imaging (MRI) is the currently preferred method and the gold standard for the structural evaluation of cartilage injuries because it allows multiplanar imaging and exhibits high soft-tissue contrast resolution [1,2]. However, MRI also exhibits a moderate detection sensitivity (64–70%) of clinically relevant (grades III and IV) articular cartilage damages [3]. Moreover, the validation and standardization of MRI sequences in the clinical routine are inconsistent, and the correlation between the results of radiological and clinical observations of cartilage injuries is debatable [4–7]. In recent years, considerable effort was made to improve cartilage MRI through the development of advanced sequences and approaches. In particular, the intra-articular administration of contrast agents for delayed MRI is a promising technology that may help to increase the efficiency of cartilage injury detection while avoiding possible systematic errors caused by intravenous contrast applications [8–10]. By intra-articularly injecting a dilute solution of a contrast agent, cartilage visualization can be significantly enhanced due to the high contrast between the cartilage and the injected fluid [11]. However, the clinically used T1 contrast agents of gadolinium chelates (including Magnevist or gadolinium(III)-

Peer review under responsibility of KeAi Communications Co., Ltd.
* Corresponding author. Orthopedic Centre, Clinical Research Centre, Zhujiang Hospital, Southern Medical University, Guangzhou, Guangdong, 510280, China.
** Corresponding author.
E-mail addresses: oayul@163.com (Y. Lu), shuang6895@aliyun.com (S. Chen).

https://doi.org/10.1016/j.bioactmat.2020.05.009
Received 29 March 2020; Received in revised form 24 May 2020; Accepted 31 May 2020

diethylenetriamine-pentaacetic acid (Gd-DTPA)) exhibit a relatively small T1 relaxivity ($r1$) of 3.3–4.3 mM^{-1} s^{-1}, which limits the detection accuracy of cartilage injuries [12–14]. Moreover, the imaging qualities of these agents remain very low because of their uniform medium distribution, and such compounds are rapidly excreted from the body through the renal system and synovial membrane of the joint capsule [15,16].

Ideally, MRI probes for cartilage injury detection should specifically bind to and penetrate the cartilage with a high $r1$ value. After imaging, they can be excreted from the body without any adverse effects. Hyaluronic acid (HA) is an essential component of the extracellular matrix (ECM) of various human tissues, including skin, connective and neural tissues, and cartilage matrix [17]. It consists of repetitive units of D-glucuronic acid and D-N-acetylglucosamine and represents the only non-sulfated glycosaminoglycan that has the same chemical composition found in different biological species. In a damaged cartilage layer, HA can bind to the articular cartilage matrix and fill the damaged collagen network [18]. The intra-articular injection of HA has been widely used in clinical applications and proven safe for osteoarthritis treatment. Furthermore, HA can increase the $r1$ values of contrast agents and prolong their accumulation in tissues because of its rigid structure, containing covalent bonds, and longer molecular rotational correlation time [19,20]. Recently, several HA-conjugated Gd chelates have been developed to enhance the MRI. For example, Guo et al. prepared dendronized-HA-tetraazacyclododecane-1,4,7,10-tetraacetic acid-Gd that exhibits high sensitivity in tumor diagnosis [21]. Another study showed that Gd-DTPA-HA could improves the quality of MRI of hepatic metastasis obtained *in vivo* [22]. Gd-DTPA-HA nanospheres with a size of approximately 250 nm were also synthesized for the specific MRI of the lymphatic system [23]. However, to the best of our knowledge, the use of such MRI probes for cartilage injury detection are very scarce. It was also assumed in previous studies that nanoparticles (NPs) can easily penetrate the healthy cartilage ECM while the movement of larger particles is hindered [24–26]. Thus, the described HA-conjugated Gd probes may not be suitable for cartilage imaging. Although some researchers utilized small size superparamagnetic iron oxide NPs to enhance the cartilage MRI, they were mostly used for stem cell labeling or the contrast enhancement of synovial tissues via phagocytosis of circulating NPs by reticuloendothelial cells instead of the direct detection of the cartilage [27–32]. Hence, MRI probes with optimal sizes, high cartilage affinities, and enhanced contrast properties should be developed for cartilage injury detection.

For this purpose, we synthesized Gd-HA NPs using a facile freeze-drying method. The resultant NPs had a sphere-like morphology with a size of approximately 50 nm. The *in vitro* T1 relaxivity of Gd-HA NPs was 3.22 and 1.49 times higher than those of clinically used Gd-DTPA and Gd-DTPA-HA, respectively. We found that Gd-HA NPs could fully penetrate the cartilage and achieved a significant enhancement of the MR images of the injured cartilage site, via an intra-articular injection of these NPs into the knee of a cartilage injury rabbit model (Fig. 1). Moreover, Gd-HA NPs demonstrated negligible influences in the blood and liver and kidney functions and were excreted from the body in urine. Therefore, the synthesized NPs can serve as an efficient and safe MRI contrast agent for the accurate cartilage injury detection.

2. Experimental section

2.1. Materials

Sodium hyaluronate was purchased from Bloomage Freda Biopharm Co. Ltd. (Shandon, China). Diethylenetriaminepentaacetic dianhydride (DTPAA) was obtained from Energy Chemical (Shanghai, China). Dimethyl sulfoxide (DMSO) was purchased from Sangong Biotech Co. Ltd. (Shanghai, China). 5-carboxyfluorescein N-succinimidyl ester (5-FAM) was purchased from Amyjet Scientific (Wuhan, China). DTPA-Gd (Magnevist, gadopentetate dimeglumine) was acquired from Bayer HealthCare Pharmaceuticals (USA). Gadolinium chloride hexahydrate ($GdCl_3{\cdot}6H_2O$) was obtained from Sigma-Aldrich (USA). All chemicals were analytical grade reagents and used without further purification.

2.2. Preparation of Gd-HA NPs

First, Gd-DTPA-HA composite was synthesized according to a previously developed procedure with some modifications [22,23,33]. Briefly, sodium hyaluronate (200 mg, 0.5 mM, MW = 990,000 Da) was dissolved in 20 mL of double distilled water (dd H_2O) and stirred for 30 min. After that, DTPAA (90 mg, 0.25 mM) solution in 600 μL DMSO was added to the reaction mixture and stirred for another 2 h. Finally, $GdCl_3{\cdot}6H_2O$ (105 mg, 0.25 mM) was added to the mixture and stirred for an additional 1 h to obtain Gd-DTPA-HA composite. After 24 h of dialysis in dd H_2O followed by a standard freeze-drying procedure [34–36], Gd-HA NPs were produced. In addition, various Gd-DTPA-HA composites were synthesized using HAs with different molecular weights (MW = 390,000, 740,000, 990,000, and 1410,000 Da) by following the same protocol.

2.3. Characterization of Gd-HA NPs

Gd-HA NPs were suspended in ethanol and placed onto a carbon-coated copper grid. Their morphology was observed by high-resolution transmission electron microscopy (TEM, JEOL 2100, Japan). Gd(III) contents of Gd-HA NPs were measured by inductively coupled plasma mass spectrometry (ICP–MS, Agilent 7900, Tokyo, Japan). Fourier transform infrared (FTIR) spectra of Gd-DPTA, HA, and Gd-DPTA-HA were recorded by an infrared spectrometer (Nicolet iS5, Thermo Fisher Scientific, USA). Hydrogen-1 nuclear magnetic resonance (^{1}H–NMR) analyses were performed using an NMR spectrometer (Bruker Avance 500 MHz equipped with 5 mm BBFO plus smart probe). The hydrodynamic diameter and zeta potential of Gd-HA NPs were measured by using Zetasizer Nano ZS 90 (Malvern Instruments, Malvern, UK). To test the stability of the prepared NPs, we suspended Gd-HA NPs in simulated body fluid (SBF) and incubated them at 37 °C. At day 0, 1, and 3, the zeta potential and hydrophilic size measurements were used to determine the changes in their surface charge and size. The release of Gd of the NPs in different conditions was performed by immersing the NPs in dd H_2O, PBS, and SBF at 25 °C and 37 °C. At day 1, 3, and 7, the samples were centrifuged, and the supernatants were tested using ICP–MS.

2.4. T1 relaxivity measurements in vitro

In vitro T1 relaxivity of the produced NPs was assessed using an MRI scanner (GE Discovery, 3T, GE Medical System, USA) with an 8-channel phased-array coil at room temperature of 25 °C. Gd-HA NPs were diluted in dd H_2O with various Gd(III) concentrations (0.0005–0.06 mM). Gd-DPTA-HA and clinically used MRI contrast agent Gd-DPTA were utilized as controls. To obtain T1-weighted images, the following parameters and sequences were employed: inversion time (TI) = 50, 100, 200, 500, 800, 1200, and 1500 ms; echo time (TE) = 8 ms; repetition time (TR) = 5000 ms; matrix dimensions = 128 × 256; bandwidth = ± 125 kHz; number of excitations = 3; and echo train length = 8. Plots of 1/relaxation time (1/T1, s^{-1}) *versus* Gd(III) concentration were constructed to obtain relaxivity values ($r1$) as their slopes. The images were analyzed on a pixel-by-pixel basis by performing a single exponential fit through the Research-T1 mapping module of a GE AW 4.6 Workstation.

2.5. Cytotoxicity assay

Cytotoxicity of Gd-HA NPs was determined using standard 3-(4,5)-dimethylthiahiazo (-z-y1)-3,5-diphenytetrazoliumromide (MTT) assay. Murine fibroblast cells (L929), human umbilical vein endothelial cells

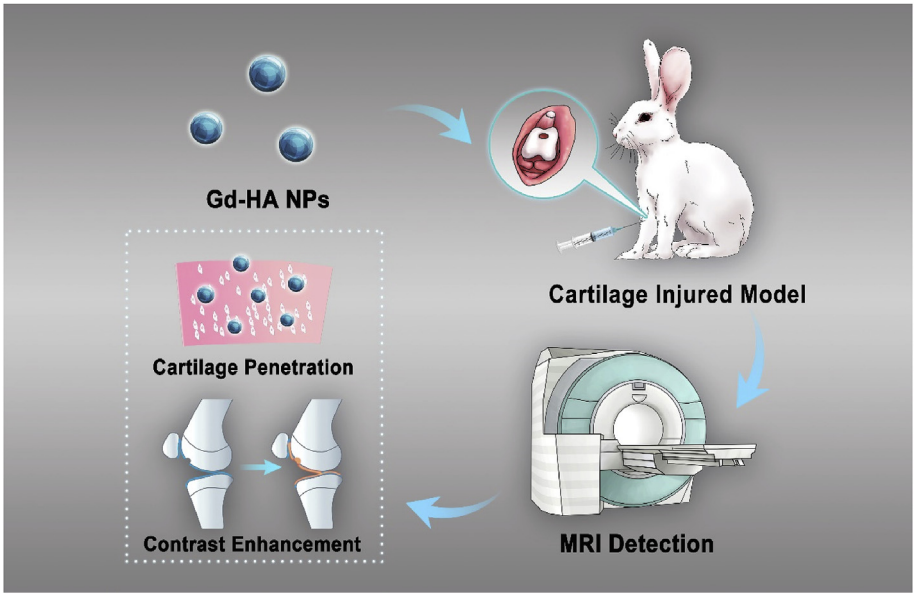

Fig. 1. Schematic diagram of the application of Gd-HA NPs in the MRI detection of cartilage injuries.

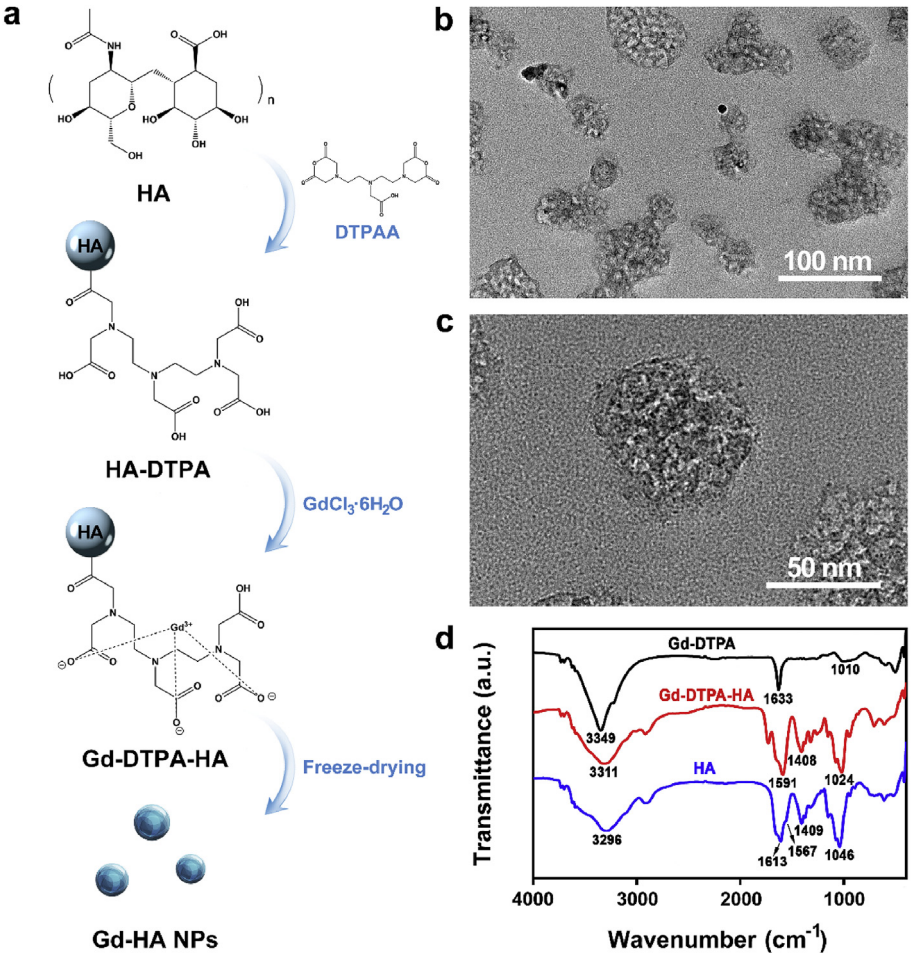

Fig. 2. Preparation and Characterization of Gd-HA NPs. (a) Schematic illustration of the fabrication of Gd-HA NPs. Gd-DPTA-HA composite was synthesized and then freeze-dried to form Gd-HA NPs. (b, c) TEM images of the as-prepared Gd-HA NPs. (d) FTIR spectra of Gd-DTPA, Gd-DTPA-HA, and HA.

(HUVEC), murine preosteoblasts (MC3T3-E1), and murine chondroprogenitor cells (ATDC5) were seeded in 96-well plates at a density of 5,000 cells per well and cultured with Dulbecco's modified Eagle's medium (DMEM, Gibco, USA) containing 10% fetal bovine serum (FBS, Gibco, USA) under 5% CO_2 atmosphere at 37 °C. After 24 h of incubation, the cells were cocultured with Gd-HA NPs at various Gd(III) concentrations (0, 0.01, 0.02, 0.05, 0.1, 0.2, and 0.4 mM) for additional 24 h. Afterwards, the media were discarded, and 200 μL of MTT

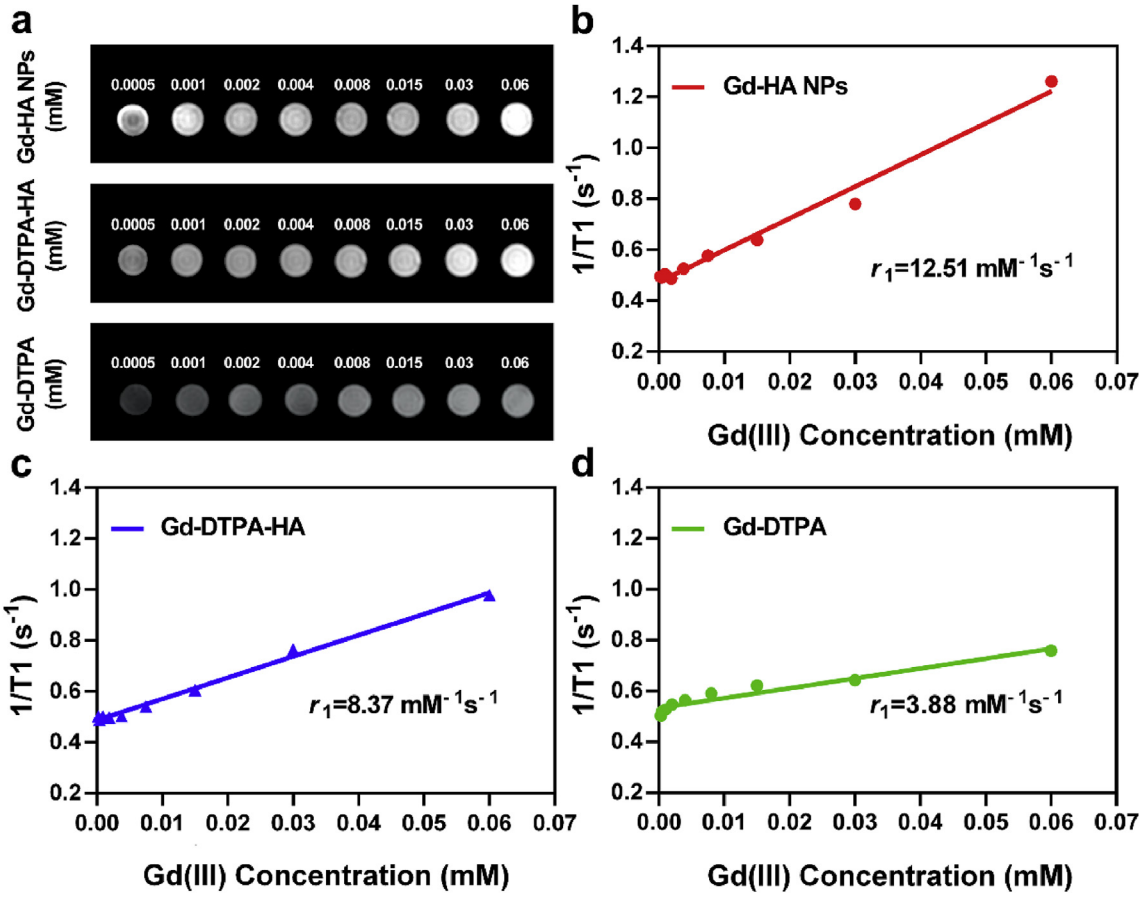

Fig. 3. *In vitro* T1-weighted MRI enhancement property of Gd-HA NPs. (a) T1 weighted MR images of Gd-HA NPs (top), Gd-DTPA-HA (middle), and Gd-DTPA (bottom) with different Gd(III) concentrations. Linear plots of the relaxation rate (1/T1) *versus* the Gd(III) concentration constructed for (b) Gd-HA NPs, (c) Gd-DTPA-HA, and (d) Gd-DTPA. The *r*1 values of Gd-HA NPs, Gd-DPTA-HA, and Gd-DTPA were 12.51, 8.37, and 3.88 $mM^{-1}\ s^{-1}$, respectively. These results indicated that Gd-HA NPs exhibited strong MRI enhancement properties.

solution (0.05%) was added to the cells, which were incubated for another 4 h. DMSO was used to dissolve formazan crystals, and optical densities (OD) were determined at a wavelength of 490 nm using a microplate reader (Multiskan GO, Thermo Scientific). Each experiment was performed in triplicate.

2.6. Live/dead cell staining

L929, HUVEC, MC3T3-E1, and ATDC cells were seeded in a 48-well cell plate and cultured for 24 h. Subsequently, Gd-HA NPs (0.4 mM) were added to the cells, which were then incubated for additional 24 h. After removing the supernatant, the cells were washed with PBS twice, and 200 μL Calcein AM and propidium iodide (BestBio, China) were added to the cell culture followed by the incubation for another 30 min at room temperature. The cells were visualized under a fluorescence microscope (DMI4000, Leica, Germany).

2.7. Hemolysis test

Healthy human blood was diluted with PBS at a ratio of 4:5 by volume. Gd-HA NPs with various Gd(III) concentrations (0.01, 0.02, 0.05, 0.1, 0.2, and 0.4 mM) were suspended in PBS and incubated at 37 °C for 30 min. PBS and dd H_2O were used as the negative and positive controls, respectively. After incubation, 200 μL of diluted blood was added into each sample and incubated at 37 °C for 1 h. All samples were centrifuged at 3000 rpm for 5 min, and OD values of the supernatant were measured at a wavelength of 545 nm using the microplate reader.

2.8. Articular cartilage injury model

Animals were purchased from the Chedun experimental animal breeding farm (Shanghai, China). Testing protocol was approved by the Institutional Animal Care and Use Committee of Huashan Hospital, Fudan University. We established an articular cartilage injury model using the results of previous studies with some modifications [37–39]. New Zealand white rabbits (male, ~3 kg) were operated under general anesthesia. First, their knees were shaved and sterilized, after which a medial parapatellar (2-cm) incision was made, and the patella was dislocated laterally. A cartilage injury (diameter: 5 mm) was made mechanically with a hollow trephine at the center of the femoral condyle, and the joint capsule, soft tissue, and skin were carefully closed. All animals received daily injections of 800,000 U of penicillin for 3 days and were allowed free movement post-operatively.

2.9. In vivo MRI detection of cartilage injuries

The established cartilage injury rabbit models (n = 5 per group) were anesthetized by sevoflurane, and Gd-HA NP aqueous solution (0.08 mM/kg) was subcutaneously injected into their knees. Gd-DTPA-HA and clinically used Gd-DPTA with the same concentrations were utilized as control groups. After that, the knees were imaged by a Siemens Verio 3T MRI system (Siemens Healthcare AG, Erlangen, Germany) equipped with a rabbit knee coil. Sagittal three-dimensional volumetric interpolated breath hold examination sequence (3D VIBE) with water-excited fat suppression was used for a contrast-enhanced imaging study with the following parameters: TR = 11.3 ms,

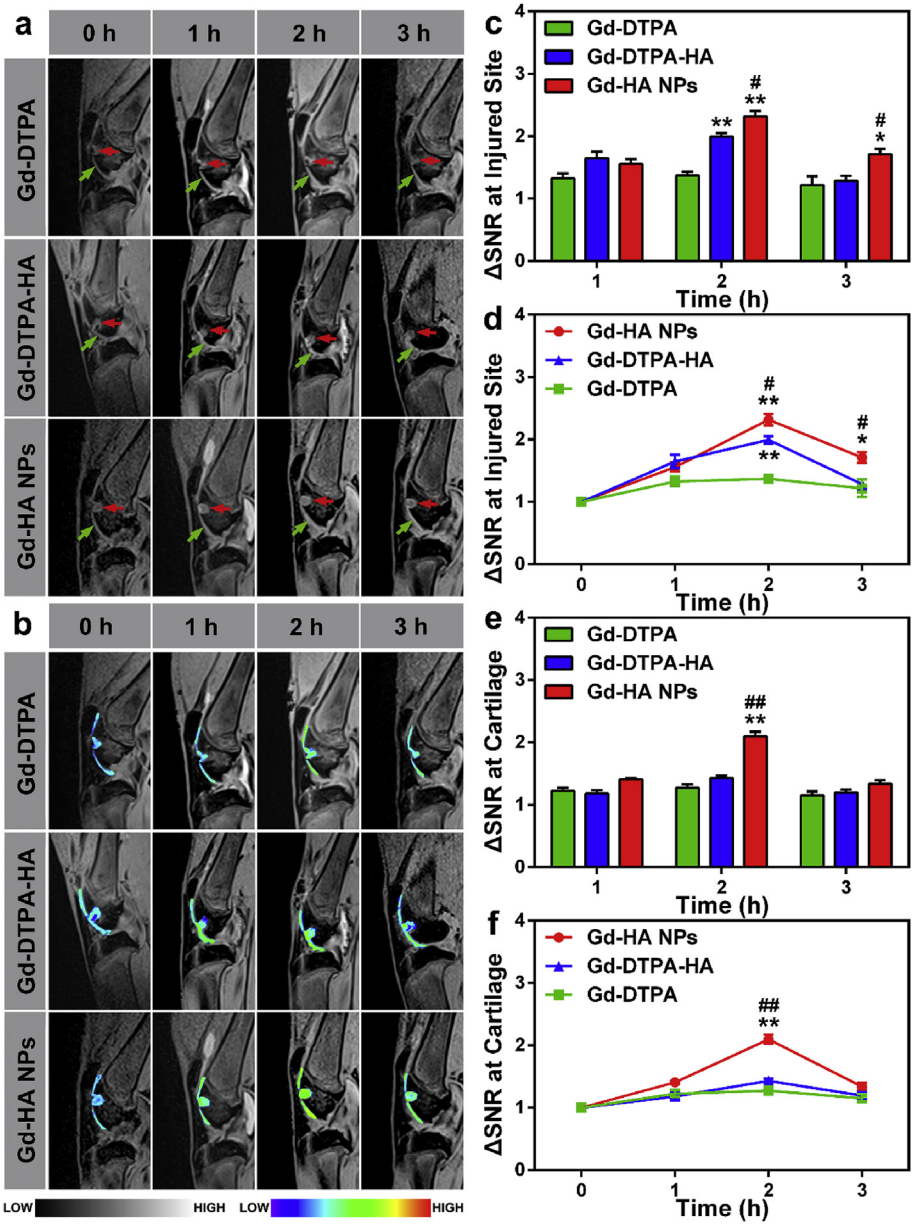

Fig. 4. *In vivo* MRI detection of cartilage injuries by Gd-HA NPs. (a) T1-weighted MRI images of the knee of the cartilage-injured rabbit obtained before and after the intra-articular injections of Gd-DTPA (top), Gd-DTPA-HA (middle), and Gd-HA NPs (bottom). The cartilage and injured site were denoted by the green and red arrows, respectively. (b) Corresponding pseudo-colored images of the cartilage and injured site obtained from the grey scale images in panel (a). (c, d) ΔSNR changes obtained from the T1-weighted MRI images of the injured site (c, d) and cartilage (e, f). These results suggested that Gd-HA NPs could significantly improve the MR imaging quality especially at the cartilage injured site. Data were presented as mean ± SEM (n = 5 per group). *p < 0.05, **p < 0.01 compared to the Gd-DTPA group; #p < 0.05, ##p < 0.01 compared to the Gd-DTPA-HA group. (For interpretation of the references to color in this figure legend, the reader is referred to the Web version of this article.)

TE = 4.9 ms, field of view = 101 × 120 mm, slice thickness = 0.8 mm, number of slices = 60, matrix dimensions = 432 × 512, resolution = 0.23 × 0.23 × 0.8 mm, number of averages = 2, pixel bandwidth = 268, and acquisition time = 3 min and 17 s. MR images were captured before and after the intra-articular injection of the contrast agents at four different time points (0, 1, 2, and 3 h). The signals within the regions of interest (ROIs; ~0.15 cm^2) were detected. The relative MRI contrast enhancement of the signal-to-noise ratio (SNR) was defined as ΔSNR = (St/Sm)/(St_0/Sm_0), where St/Sm was the signal ratio of ROI to the surrounding muscle in the post-contrast MR images, and St_0/Sm_0 was the signal ratio of ROI to the surrounding muscle in the pre-contrast images. The trend of signal changes was determined by plotting ΔSNR *versus* time. All measurements were performed on a PACS workstation (Horos version 3.3.6, USA) and Syngo MR B19 system (Siemens Healthcare AG, Erlangen, Germany). After MR imaging, the rabbits were sacrificed, and their femoral condyles were collected. The obtained samples were fixed in 4% formalin solution overnight, decalcified in ethylene diamine tetraacetic acid solution, embedded in paraffin, and cut into various sections, which were subjected to hematoxylin and eosin (H&E) staining, safranin O-fast green staining, and periodic acid-Schiff (PAS) staining.

2.10. Cartilage binding ability of Gd-HA NPs in vivo

The rabbits were intra-articularly injected with 5-FAM-labeled Gd-HA NPs or 5-FAM-labeled Gd-HA-DTPA (0.08 mM/kg). After 2 h post-injection, the cartilage of the joint was collected and cut into slices, which were subsequently imaged under a fluorescence microscope (BX51, Olympus, Japan). 4′,6′-diamidino-2-phenylindole was used for nucleus staining.

2.11. Biocompatibility and metabolism of NPs in vivo

Kunming mice (male, ~25 g) were purchased from Shanghai Laboratory Animal Center Co. Ltd. (Shanghai, China) for *in vivo* biocompatibility and biodistribution studies. Mice (n = 12) were intra-articularly injected with Gd-HA NPs (0.08 mM/kg), and their body temperatures and weights were recorded after 0, 3, 12, and 24 h, and after 2, 3, 4, 5, 6, and 7 days. At day 1, 3, and 7 post-injection, the mice in the Gd-HA group (n = 4 at each time interval) were sacrificed, and

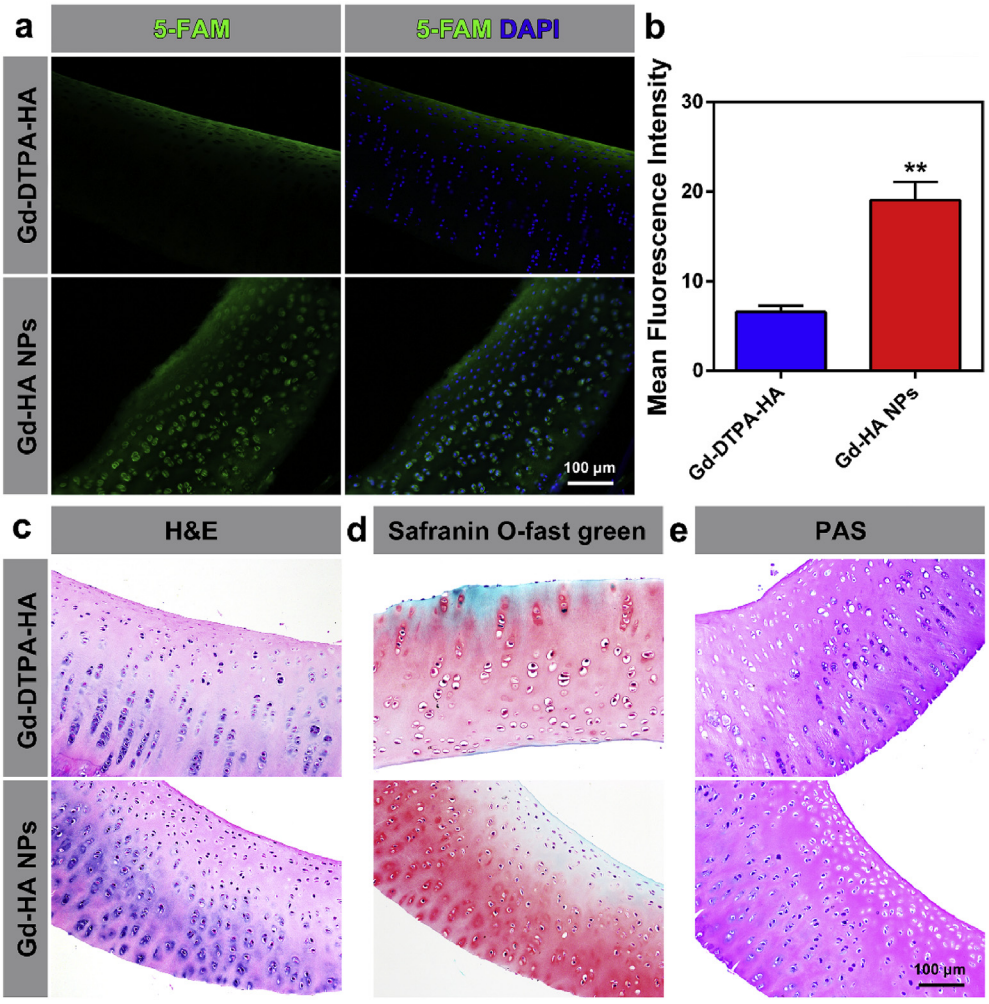

Fig. 5. Affinity and histocompatibility of Gd-HA NPs towards the cartilage. (a) Fluorescent images of the cartilage obtained after 2 h of post-injection for the 5-FAM-labeled Gd-DTPA-HA (top) and Gd-HA NPs (bottom). Strong fluorescence was observed throughout the full cartilage thickness in the Gd-HA NP group. (b) Fluorescent semi-quantification of 5-FAM in the cartilage performed after different treatments. Results of (c) H&E, (d) safranin O-fast green, and (e) PAS cartilage staining obtained after the injections of various contrast agents. Data were presented as mean ± SEM (n = 5 per group). *p < 0.05, **p < 0.01 compared to the Gd-DTPA-HA group. (For interpretation of the references to color in this figure legend, the reader is referred to the Web version of this article.)

their main organs including hearts, livers, lungs, kidneys, and spleens were collected and dissolved in aqua regia. The blood, urine, and feces of these mice were collected as well. Gd contents of the samples were determined by ICP–MS. In addition, H&E staining was performed to monitor the histological changes of the main organs. Blood routine tests were conducted with a Sysmex XT-1800i hematology analyzer (Sysmex Corporation, Kobe, Japan). Levels of alanine aminotransferase, aspartate aminotransferase, alkaline phosphatase, γ-glutamyl transferase, blood urea nitrogen, and creatinine in the serum were obtained with a FUJIFILM DRI-Chem 7000i clinical chemistry analyzer (Fujifilm Corporation, Tokyo, Japan). The mice (n = 4) without injections served as the normal control (NC) group.

2.12. Statistical analysis

The obtained data were analyzed using SPSS 22.0 software (IBM, USA). Statistical comparisons were performed via one-way analysis of variance followed by post-hoc multiple comparison (Turkey's test). Results of the *in vitro* and *in vivo* studies were presented as means ± standard deviation and means ± standard error of mean (SEM), respectively. A level of $p < 0.05$ was defined as statistically significant.

3. Results and discussion

3.1. Preparation and characterization of Gd-HA NPs

Gd-HA NPs were synthesized using the facile method illustrated in Fig. 2a. First, HA-DTPA was formed from the hydroxy groups of HA and carboxyl groups of DTPAA via a ring-opening reaction. After that, HA-DPTA was crosslinked by $GdCl_3{\cdot}6H_2O$ to produce a Gd-DTPA-HA composite, which subsequently underwent a freeze-drying procedure to obtain Gd-HA NPs. As shown in Fig. S1 in the Electronic Supplementary Material (ESM), Gd-DTPA-HA species have irregular shapes with sizes of several micrometers. After freeze-drying, Gd-HA NPs with sizes of approximately 50 nm were formed (Fig. 2b and c). The dynamic light scattering (DLS) result showed the hydrophilic size of Gd-HA NPs to be ~70 nm, and the zeta potential value was −19.2 mV (Fig. S2 in the ESM). The Gd(III) content in these particles, determined by ICP–MS, was 0.193 mg/g. Thus, 57.7% of Gd(III) was chelated into HA-DTPA considering that the reaction molar ratio between HA-DTPA and Gd(III) was 1:0.8, which indicated that approximately six DTPA molecules were embedded into a single HA chain.

The successful conjugation of Gd with HA-DTPA was also confirmed by FTIR. As illustrated in Fig. 2d, HA characteristic absorption peaks corresponding to C=O (amide I) and C–N (amide II) species were observed at 1613 and 1567 cm^{-1}, respectively. The bands at 1409 and 1046 cm^{-1} were attributed to C–O and N–H stretching vibrations, respectively [40]. The main characteristic absorption peak of Gd-DTPA was centered at 1633 cm^{-1}. Compared to pure Gd-DTPA, Gd-DTPA-HA exhibited the characteristic peaks of both HA and Gd-DPTA. Moreover, the main Gd-DTPA peaks centered at 1633 and 1010 cm^{-1} shifted to 1591 and 1024 cm^{-1} in the case of Gd-DTPA-HA, respectively, and their intensities increased because of the increase in the intensities of the C–N and N–H HA vibrations [23]. ^{1}H–NMR analyses were performed to further confirmed the chelation of HA-DTPA-Gd. The chelate reaction between Gd(III) and sidechain of DTPAA produced a

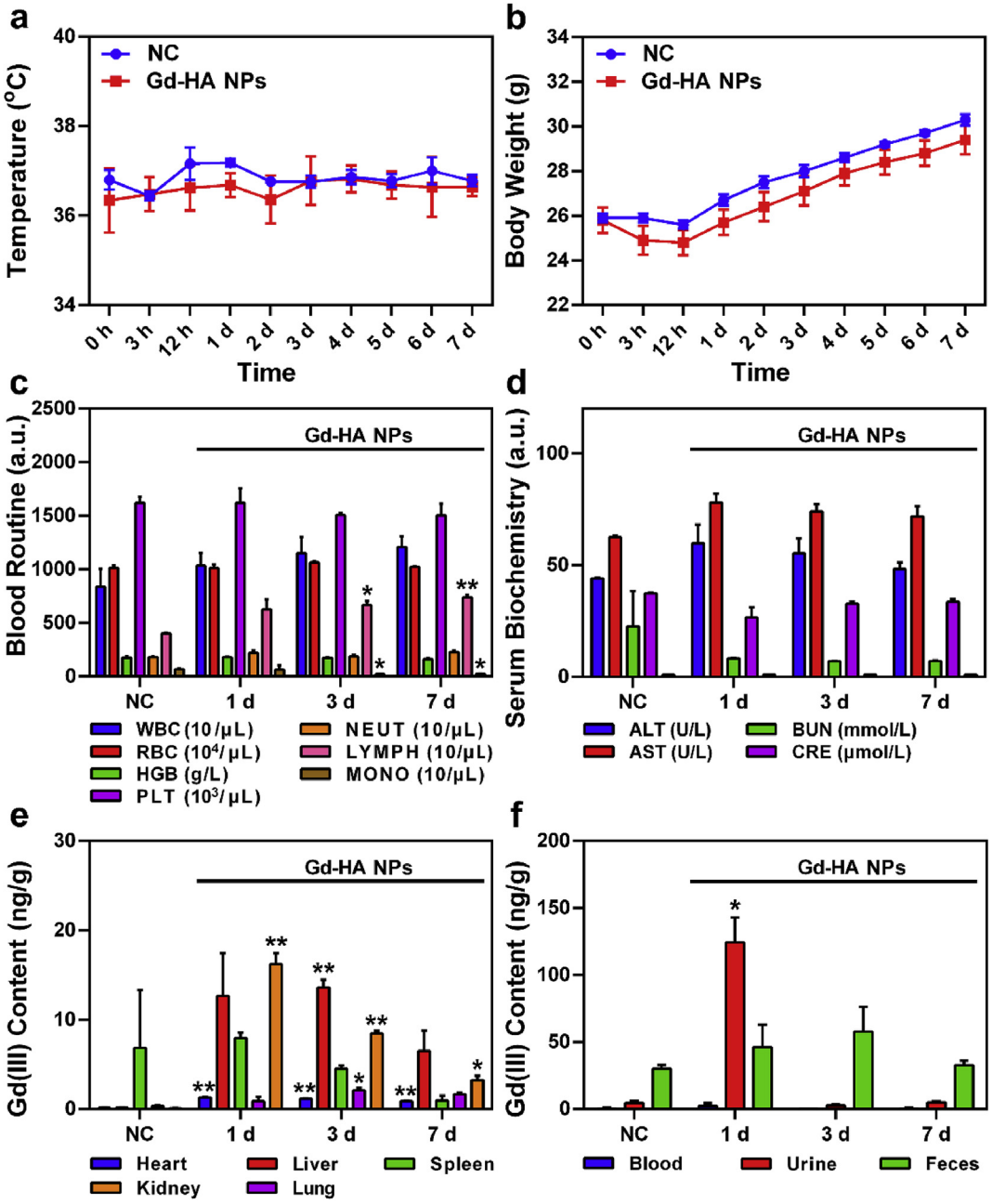

Fig. 6. *In vivo* safety and metabolism of Gd-HA NPs. Changes in the (a) body temperature and (b) body weight observed for the NC and Gd-HA NP groups during 7 d of post-injection. (c) Blood routine assay and (d) results of the serum biochemical testing (d) of the mice injected with Gd-HA NPs. (e, f) Biodistributions of Gd(III) ions in the mice obtained at day 1, 3, and 7 post-injection of Gd-HA NPs. Data were presented as mean ± SEM (n = 5 per group). *p < 0.05, **p < 0.01 compared to the NC group.

deshielding effect that protons (–CH_2–) between carbonyl and tertiary amine shifted to the lower field (Fig. S3 in the ESM).

Moreover, we tested the stability of Gd-HA NPs by incubating them in SBF at 37 °C. The DLS results (Fig. S4a in the ESM) showed that the size of Gd-HA NPs was ~70 nm at day 0 and day 1, following which, the size slightly increased to ~90 nm at day 3. Moreover, the zeta potential of the NPs exhibited negligible changes during incubation (Fig. S4b in the ESM). These results suggested that Gd-HA NPs were stable. The release of Gd in different solutions was also tested over 7 days (Fig. S5 in the ESM). The results showed that no more than 7% of Gd leaked from the NPs, suggesting that NPs are safe as contrast agents.

3.2. *In vitro* MRI relaxivity of Gd-HA NPs

To investigate the potential application of Gd-HA NPs as an MRI probe, we measured their longitudinal relaxivity value ($r1$) using the MRI scanner. As shown in Fig. 3a and Table S1 in the ESM, Gd-HA NPs and Gd-DTPA-HA exhibited close signal intensities, which increased with increasing Gd(III) concentrations. However, clinically used Gd-DTPA demonstrated no apparent signal changes within the experimental concentrations. The signal intensities of NPs and Gd-DTPA-HA were greater than those of clinical Gd-DTPA at close Gd(III) concentrations. Furthermore, the $r1$ values of Gd-HA NPs and Gd-DTPA-HA were 12.51 and 8.37 mM^{-1} s^{-1}, respectively, whereas that of Gd-DTPA was 3.88 mM^{-1} s^{-1} (Fig. 3b–d). These results suggest that the synthesized NPs can detect articular cartilage injuries more accurately than

the commercial contrast agent. The rotational correlation time and water exchange rate are the major factors that influence the $r1$ value of contrast agents. Slower rotational correlation time and the higher water exchange rates for the agents, result in the stronger $r1$ values [19]. Because of both hydrophilic and hydrophobic properties, HA molecules can form a continuous three-dimensional cellular network structure, in which the water exchange rate increases [41]. Moreover, HA increases the molecular weight of the Gd chelate, resulting in a slower rotational correlation time [19]. These features of HA enhance the T1 signal intensity of Gd-DTPA-HA and Gd-HA NPs as compared to that of Gd-DTPA.

Additionally, the increase in the molecular weight of HA will result in slower rotational correlation time accompanied by a higher $r1$ value. However, the correlation between the $r1$ value and MW is nonlinear [19]. Thus, $r1$ values were determined for the Gd-DTPA-HA composites produced from HAs with different molecular weights (MW = 390,000, 740,000, 990,000, and 1410,000 Da). All magnitudes exceeded the $r1$ value obtained for Gd-DTPA. Furthermore, Gd-DTPA-HA synthesized from HA with a molecular weight of 990,000 Da possessed the highest $r1$ value (Fig. S6 and Table S1 in the ESM) and, therefore, it was selected as the most suitable HA compound in this study. We also prepared Gd-HA NPs with different sizes (~25 and ~200 nm) and evaluated their T1 imaging properties. As presented in Fig. S7 in the ESM, the $r1$ values of Gd-HA NPs were similar. Considering the $r1$ value of our prepared NPs and the fact that NPs larger than 96 nm could barely penetrate the cartilage surface [25], Gd-HA NPs with a size of 50 nm were chosen for further study.

3.3. In vivo MRI enhancement of cartilage defects by Gd-HA NPs

Gd-HA NPs, Gd-DTPA-HA, and Gd-DTPA were intra-articularly injected into the knee of the cartilage injury rabbit model. After the injection, the knee was imaged with the Siemens Verio 3T MRI system equipped with a rabbit knee coil. As shown in Fig. 4a and b, the articular cartilage (indicated by the red dotted lines) and damaged area (indicated by the blue dotted lines) were not clearly observed in both groups before the injections of the contrast agents. After 1 h of the intra-articular injection of Gd-DTPA, the signal intensity of the whole articular cavity increased; however, the lesion image was only slightly enhanced, and the cartilage contours remained unclear. At 2 and 3 h post-injection, the signal intensities of the cartilage and injured sites remained very close. In contrast, 1 h after the injection, many intense signals were detected at the cartilage and injured site for the Gd-DTPA-HA and Gd-HA NP groups. Moreover, the MRI signals obtained for the cartilage and lesion became much stronger at 2 h post-injection. We also observed that the intensities of MRI signals slightly decreased 3 h after the injection, indicating that the contrast agents started to get metabolized, which was in good agreement with the appropriate MRI time window of 2–3 h established for cartilage assessment [42,43].

In addition, SNR values were determined from the T1-weighted MRI images of the cartilage and injured site. As expected, the Gd-HA NP group demonstrated a significantly higher ΔSNR magnitude at the injured site as compared to that in the Gd-DTPA-HA and Gd-DTPA groups (Fig. 4c and d). The ΔSNR values measured for the Gd-DTPA group fluctuated at approximately 1.3, indicating that the signals generated by these lesions were affected by the administration of clinically used Gd-DTPA only slightly. Remarkably, the ΔSNR of the lesions increased by a factor of 2.3 at 2 h post-injection of Gd-HA NPs and remained significantly higher than that in the Gd-DTPA-HA and Gd-DTPA groups at 3 h post-injection. In addition, NPs also enhanced the obtained cartilage images, whereas the ΔSNR values of the Gd-HA NP group were very close to those of the Gd-DTPA-HA group (Fig. 4e and f). Hence, the synthesized Gd-HA NPs were more sensitive to cartilage injuries than the other two contrast agents and could indeed enhance detection by MRI.

To identify the reason for the superior MRI enhancement properties of Gd-HP NPs, the affinities of the studied contrast agents to the cartilage were determined. At 2 h post-injection of the fluorescent 5-FAM-labeled Gd-DTPA-HA, green fluorescence was only observed on the cartilage surface (Fig. 5a). In contrast, in the 5-FAM-labeled Gd-HA NP group, strong fluorescence was detected over the entire cartilage thickness. Note that fluorescence in the Gd-HA NPs group was observed even for the cartilage lacuna, suggesting that Gd-HA NPs could penetrate the cartilage depth to improve the MR imaging quality. Additionally, H&E, safranin O-fast green, and PAS staining procedures were performed on the cartilage after the injection. As compared to that in the healthy controls (Fig. S8 in the ESM), the results of H&E and safranin O-fast green staining showed that the cartilage in both the Gd-DPTA-HA and Gd-HA NP groups exhibited no damage or inflammation after the exposure to the contrast agents (Fig. 5c and d, and S8 in the ESM). Meanwhile, the cartilage in these groups turned purplish-red after PAS staining because of the presence of oligosaccharides of glycoproteins or other structural proteins, indicating that Gd-HA NPs did not exert any adverse effects on the cartilage structure or composition (Fig. 5e and S8 in the ESM). These results demonstrated that the synthesized NPs could serve as an efficient MRI contrast probe to detect cartilage injuries *in vivo*.

3.4. Biosafety and metabolism of Gd-HA NPs

As contrast agents containing Gd(III) chelates for clinical applications, the majority of MRI agents reach normal tissues after injection. Their potential metabolic toxicity to normal cells and organs results from the possibility of chelate dissociation, which produces Gd(III) species [14,15,44]. Moreover, although the intravenous administration of Gd-DTPA was found to be secure, the safety of the intra-articular application of Gd-based contrast agents has not been studied in detail [15]. Hence, in this work, we determined the biocompatibility of Gd-HA NPs both *in vitro* and *in vivo*.

To evaluate the cytotoxicity of Gd-HA NPs, a standard MTT assay was performed on L929, HUVEC, MC3T3-E1, and ATDC5 cell lines after coculturing with NPs for 24 h. As shown in Fig. S9 in the ESM, no significant cytotoxicity was observed for any of the cell lines even at Gd (III) concentrations of Gd-HA NPs as high as 0.4 mM. Moreover, the results of the live/dead staining procedure (Fig. S10 in the ESM) showed that the cells cocultured with Gd-HA NPs (40 mM) maintained their typical morphology. Most cells were alive (green fluorescence), and very few dead cells were detected (red fluorescence), suggesting that Gd-HA NPs exhibited negligible cytotoxicity toward the normal cells. In addition, hemolysis with NPs was examined. As shown in Fig. S11 in the ESM, the supernatants of the NP and PBS (negative control) groups were transparent, whereas those of the dd H_2O (positive control) group turned red due to the release of hemoglobin from the broken red blood cells. The results of quantitative analysis revealed that OD values between the NP and PBS groups were not significantly different, demonstrating that Gd-HA NPs were safe for blood components.

Additional studies on the *in vivo* safety and metabolism of Gd-HA NPs involved their articular injection into mice. After administering NPs or normal saline (serving as the NC group), changes in the mouse body temperature, behavior, and body weight were determined. As shown in Fig. 6a, the body temperatures of the mice in both groups exhibited no significant fluctuations over the period from 0 h to 7 days. In addition, no abnormal changes in the body weight as compared to those in the NC group were detected (Fig. 6b). The observed steady increase in body weight indicated that Gd-HA NPs did not induce adverse effects on mouse growth. Moreover, as compared to those in the NC group, the mice injected with Gd-HA NPs did not show apparent signs of anorexia, locomotor impairment, dehydration, muscle loss, or other signs associated with animal toxicity and mortality during 7 days of observation.

Histological analysis was performed to evaluate possible side effects of Gd-HA NPs or the influence of their degradation products on normal

organs (Fig. S12 in the ESM). The main organs of the mice exposed to Gd-HA NPs exhibited no signs of damage, inflammation, or lesion formation as compared to that observed in the NC group. In addition, routine blood testing (Fig. 6c) showed that NPs only slightly influenced the number of monocytes and lymphocytes that remained within their normal ranges. Serum biochemistry results (Fig. 6d) indicated the absence of significant differences between the Gd-HA NP and NC groups suggesting that NPs should not affect the blood system or liver and kidney functions.

Generally, the high number and long-term retention of Gd-based NPs in the body might lead to the development of undesirable diseases induced by Gd(III) ions [15]. To further evaluate the metabolism of Gd-HA NPs *in vivo*, Gd(III) contents in the major organs of the mice were measured at day 1, 3, and 7 after the articular injection of NPs. As shown in Fig. 6e, the Gd contents that accumulated in the main mouse organs were relatively low, whereas these values determined for the kidneys, livers, and spleens were higher than those obtained for the other organs. As compared to those in the NC group, much higher Gd contents were detected in the kidneys and livers suggesting that both Gd-HA NPs and the products of their degradation were mainly metabolized by these two organs. Moreover, the Gd contents in the kidneys and livers gradually decreased with time. In particular, the Gd residue in the kidney was 16.21 ng/g at day 1 and decreased to only 3.21 ng/g at day 7 post-injection. These results were consistent with metabolism of the clinical agent, Gd-DTPA [15,45]. While the relatively fast metabolism of Gd-DTPA might impair renal function, the optimal metabolism rate of the synthesized NPs might help to avoid latent side effects and minimize their potential toxicity towards the normal organs.

Finally, clearance of the produced NPs was studied. As shown in Fig. 6f, Gd urine contents in the Gd-HA NPs group were significantly higher than those in the NC group at 1 day post-injection, which confirmed that NPs could be excreted from the body with urine. Overall, we verified that Gd-HA NPs caused no adverse effects and could be cleared from the mouse body after injection, indicating their safety for the MR imaging of articular cartilage injuries.

4. Conclusions

In summary, Gd-HA NPs were developed as a novel MRI contrast agent, which exhibited good biocompatibility and high longitudinal relaxivity. Owing to their optimal size and high affinity to ECM, Gd-HA NPs can simultaneously penetrate the inner part of cartilage tissues and serve as an efficient MR imaging probe for the accurate detection of cartilage injuries. Moreover, Gd-HA NPs can be cleared by the body with urine without causing adverse effects on organ functions. Hence, these NPs can be potentially used in the clinical cartilage injury detection by MRI.

CRediT authorship contribution statement

Rong Lu: Writing - original draft, Methodology, Investigation, Validation. **Yuyang Zhang:** Validation. **Hongyue Tao:** Methodology, Investigation. **Lu Zhou:** Methodology, Investigation. **Huidi Li:** Methodology, Investigation. **Tianwu Chen:** Validation. **Peng Zhang:** Validation. **Yao Lu:** Conceptualization, Funding acquisition, Supervision, Writing - review & editing. **Shuang Chen:** Conceptualization, Funding acquisition, Supervision, Writing - review & editing.

Declaration of competing interest

None.

Acknowledgements

This work was supported by the National Natural Science Foundation of China (81671652, 81902198), National Key Research and Development Program of China (2018YFC2000205), Guangdong Basic and Applied Basic Research Foundation (2020A1515010398), China Postdoctoral Science Foundation (BX20190150, 2019M662980), President Foundation of Zhujiang Hospital, Southern Medical University (yzjj2018rc09), and Scientific Research Foundation of Southern Medical University (C1051353, PY2018N060).

Appendix A. Supplementary data

Supplementary data to this article can be found online at https://doi.org/10.1016/j.bioactmat.2020.05.009.

References

[1] D. Hayashi, F.W. Roemer, A. Guermazi, Magnetic resonance imaging assessment of knee osteoarthritis: current and developing new concepts and techniques, Clin. Exp. Rheumatol. 37 (5) (2019) 88–95 Suppl 120.
[2] E. Oei, M. Wick, A. Müller-Lutz, C. Schleich, F. Miese, Cartilage Imaging: techniques and developments, Semin. Muscoskel. Radiol. 22 (2018) 245–260, https://doi.org/10.1055/s-0038-1639471 02.
[3] J.E.J. Bekkers, A.I. Tsuchida, D.B.F. Saris, Cartilage injury, in: M. Bhandari (Ed.), Evidence-based Orthopedics, Blackwell Publishing Ltd., New Jersey, 2011(chapter 99).
[4] T.M. Link, Editorial comment: the future of compositional MRI for cartilage, Eur. Radiol. 28 (7) (2018) 2872–2873, https://doi.org/10.1007/s00330-018-5457-4.
[5] F.W. Roemer, R. Kijowski, A. Guermazi, Editorial: from theory to practice - the challenges of compositional MRI in osteoarthritis research, Osteoarthritis Cartilage 25 (12) (2017) 1923–1925, https://doi.org/10.1016/j.joca.2017.08.007.
[6] D. Hayashi, X. Li, A.M. Murakami, F.W. Roemer, S. Trattnig, A. Guermazi, Understanding magnetic resonance imaging of knee cartilage repair: a focus on clinical relevance, Cartilage 9 (3) (2018) 223–236, https://doi.org/10.1177/1947603517710309.
[7] F. Eckstein, M.-P.H. Le Graverand, Plain radiography or magnetic resonance imaging (MRI): which is better in assessing outcome in clinical trials of disease-modifying osteoarthritis drugs? Summary of a debate held at the World Congress of Osteoarthritis 2014, Semin. Arthritis Rheum. 45 (3) (2015) 251–256, https://doi.org/10.1016/j.semarthrit.2015.06.001.
[8] R.J. Kalke, G.A. Di Primio, M.E. Schweitzer, MR and CT arthrography of the knee, Semin. Muscoskel. Radiol. 16 (1) (2012) 57–68, https://doi.org/10.1055/s-0032-1304301.
[9] B. Klaan, F. Wuennemann, L. Kintzelé, A.S. Gersing, M.A. Weber, [MR and CT arthrography in cartilage imaging: indications and implementation], Radiologe 59 (8) (2019) 710–721, https://doi.org/10.1007/s00117-019-0564-z.
[10] Y. Kang, J.-Y. Choi, H.J. Yoo, S.H. Hong, H.S. Kang, Delayed gadolinium-enhanced MR imaging of cartilage: a comparative analysis of different gadolinium-based contrast agents in an ex vivo porcine model, Radiology 282 (3) (2017) 734–742, https://doi.org/10.1148/radiol.2016160367.
[11] A. Guermazi, H. Alizai, M.D. Crema, S. Trattnig, R.R. Regatte, F.W. Roemer, Compositional MRI techniques for evaluation of cartilage degeneration in osteoarthritis, Osteoarthritis Cartilage 23 (10) (2015) 1639–1653, https://doi.org/10.1016/j.joca.2015.05.026.
[12] Z. Huang, Y. Chen, D. Liu, C. Lu, Z. Shen, S. Zhong, G. Shi, Gadolinium-conjugated star-block copolymer polylysine-modified polyethylenimine as high-performance T1 MR imaging blood pool contrast agents, RSC Adv. 8 (9) (2018) 5005–5012, https://doi.org/10.1039/C7RA08820E.
[13] W. Le, S. Cui, X. Chen, H. Zhu, B. Chen, Z. Cui, Facile Synthesis of gd-functionalized gold nanoclusters as potential MRI/CT contrast agents, Nanomaterials 6 (4) (2016) 65, https://doi.org/10.3390/nano6040065.
[14] H.K. Kim, G.H. Lee, Y. Chang, Gadolinium as an MRI contrast agent, Future Med. Chem. 10 (6) (2018) 639–661, https://doi.org/10.4155/fmc-2017-0215.
[15] G. Schulte-Altedorneburg, M. Gebhard, W.A. Wohlgemuth, W. Fischer, J. Zentner, R. Wegener, T. Balzer, K. Bohndorf, MR arthrography: pharmacology, efficacy and safety in clinical trials, Skeletal. Radiol. 32 (1) (2003) 1–12, https://doi.org/10.1007/s00256-002-0595-8.
[16] K.S. Kwack, J.H. Cho, M.M. Kim, C.S. Yoon, Y.S. Yoon, J.W. Choi, J.W. Kwon, B.H. Min, J.S. Sun, S.Y. Kim, Comparison study of intraarticular and intravenous gadolinium-enhanced magnetic resonance imaging of cartilage in a canine model, Acta Radiol. 49 (1) (2008) 65–74, https://doi.org/10.1080/02841850701552934.
[17] H. Pereira, D.A. Sousa, A. Cunha, R. Andrade, J. Espregueira-Mendes, J.M. Oliveira, R.L. Reis, Hyaluronic acid, Adv. Exp. Med. Biol. 1059 (2018) 137–153, https://doi.org/10.1007/978-3-319-76735-2_6.
[18] X.L. Shang, H.Y. Tao, S.Y. Chen, Y.X. Li, Y.H. Hua, Clinical and MRI outcomes of HA injection following arthroscopic microfracture for osteochondral lesions of the talus, Knee Surg. Sports Traumatol. Arthrosc. 24 (4) (2016) 1243–1249, https://doi.org/10.1007/s00167-015-3575-y.
[19] É. Tóth, L. Helm, A.E. Merbach, Relaxivity of MRI contrast agents, in: W. Krause

(Ed.), Contrast Agents I: Magnetic Resonance Imaging, Springer Berlin Heidelberg., Berlin, Heidelberg, 2002, pp. 61–101.
[20] P.P.G. Guimaraes, S. Gaglione, T. Sewastianik, R.D. Carrasco, M.J. Mitchell, Nanoparticles for immune cytokine TRAIL-based cancer therapy, ACS Nano 12 (2) (2018), https://doi.org/10.1021/acsnano.7b05876 acsnano.7b05876.
[21] C. Guo, L. Sun, H. Cai, Z. Duan, S. Zhang, Q. Gong, K. Luo, Z. Gu, Gadolinium-labeled biodegradable dendron-hyaluronic acid hybrid and its subsequent application as a safe and efficient magnetic resonance imaging contrast agent, ACS Appl. Mater. Interfaces 9 (28) (2017) 23508–23519, https://doi.org/10.1021/acsami.7b06496.
[22] M. Moon, R.G. Thomas, S.U. Heo, M.S. Park, W.K. Bae, S.H. Heo, N.Y. Yim, Y.Y. Jeong, A hyaluronic acid-conjugated gadolinium hepatocyte-specific T1 contrast agent for liver magnetic resonance imaging, Mol. Imag. Biol. 17 (4) (2015) 497–503, https://doi.org/10.1007/s11307-014-0819-z.
[23] G. Wu, H. Zhang, Z. Zhan, Q. Lu, J. Cheng, J. Xu, J. Zhu, Hyaluronic acid-gadolinium complex nanospheres as lymphatic system-specific contrast agent for magnetic resonance imaging, Chin. J. Chem. 33 (10) (2015) 1153–1158, https://doi.org/10.1002/cjoc.201500135.
[24] R. Labens, B.D. Lascelles, A.N. Charlton, N.R. Ferrero, A.J. Van Wettere, X.R. Xia, A.T. Blikslager, Ex vivo effect of gold nanoparticles on porcine synovial membrane, Tissue Barriers 1 (2) (2013) e24314, , https://doi.org/10.4161/tisb.24314.
[25] D.A. Rothenfluh, H. Bermudez, C.P. O'Neil, J.A. Hubbell, Biofunctional polymer nanoparticles for intra-articular targeting and retention in cartilage, Nat. Mater. 7 (3) (2008) 248–254, https://doi.org/10.1038/nmat2116.
[26] K.A. Elsaid, L. Ferreira, T. Truong, A. Liang, J. Machan, G.G. D'Souza, Pharmaceutical nanocarrier association with chondrocytes and cartilage explants: influence of surface modification and extracellular matrix depletion, Osteoarthritis Cartilage 21 (2) (2013) 377–384, https://doi.org/10.1016/j.joca.2012.11.011.
[27] G.M. van Buul, G. Kotek, P.A. Wielopolski, E. Farrell, P.K. Bos, H. Weinans, A.U. Grohnert, H. Jahr, J.A. Verhaar, G.P. Krestin, G.J. van Osch, M.R. Bernsen, Clinically translatable cell tracking and quantification by MRI in cartilage repair using superparamagnetic iron oxides, PloS One 6 (2) (2011) e17001, , https://doi.org/10.1371/journal.pone.0017001.
[28] D.J. Korchinski, M. Taha, R. Yang, N. Nathoo, J.F. Dunn, Iron oxide as an MRI contrast agent for cell tracking, Magn. Reson. Insights 8 (Suppl 1) (2015) 15–29, https://doi.org/10.4137/MRI.S23557.
[29] Y.X. Wang, Superparamagnetic iron oxide based MRI contrast agents: current status of clinical application, Quant. Imag. Med. Surg. 1 (1) (2011) 35–40, https://doi.org/10.3978/j.issn.2223-4292.2011.08.03.
[30] G.H. Simon, J. von Vopelius-Feldt, M.F. Wendland, Y. Fu, G. Piontek, J. Schlegel, M.H. Chen, H.E. Daldrup-Link, MRI of arthritis: comparison of ultrasmall superparamagnetic iron oxide vs. Gd-DTPA, J. Magn. Reson. Imag. 23 (5) (2006) 720–727, https://doi.org/10.1002/jmri.20556.
[31] A. Amirabadi, L. Vidarsson, E. Miller, M.S. Sussman, K. Patil, H. Gahunia, S.A. Peel, A. Zhong, R. Weiss, G. Detzler, H.L. Cheng, R. Moineddin, A.S. Doria, USPIO-related T1 and T2 mapping MRI of cartilage in a rabbit model of blood-induced arthritis: a pilot study, Haemophilia 21 (1) (2015) e59–69, https://doi.org/10.1111/hae.12601.
[32] M. Xie, S. Luo, Y. Li, L. Lu, C. Deng, Y. Cheng, F. Yin, Intra-articular tracking of adipose-derived stem cells by chitosan-conjugated iron oxide nanoparticles in a rat osteoarthritis model, RSC Adv. 9 (21) (2019) 12010–12019, https://doi.org/10.1039/C8RA09570A.
[33] S. Gouin, M.V.V. Grayeb, F.o.M. Winnik, Gadolinium diethylene-triaminepentaacetic acid hyaluronan conjugates: preparation, properties and applications, Macromol, Symploke 186 (1) (2002) 105–110, https://doi.org/10.1002/1521-3900(200208)186:1<105::AID-MASY105>3.0.CO;2-2.
[34] W. Abdelwahed, G. Degobert, S. Stainmesse, H. Fessi, Freeze-drying of nanoparticles: formulation, process and storage considerations, Adv. Drug Deliv. Rev. 58 (15) (2006) 1688–1713, https://doi.org/10.1016/j.addr.2006.09.017.
[35] L. Qian, H. Zhang, Controlled freezing and freeze drying: a versatile route for porous and micro-/nano-structured materials, J. Chem. Technol. Biotechnol. 86 (2) (2011) 172–184, https://doi.org/10.1002/jctb.2495.
[36] J. Zhao, Y. He, L. Zhang, K. Lu, Preparation of porous TiO2 powder with mesoporous structure by freeze-drying method, J. Alloys Compd. 678 (2016) 36–41, https://doi.org/10.1016/j.jallcom.2016.03.253.
[37] Z. Chen, C. Yan, S. Yan, Q. Liu, M. Hou, Y. Xu, R. Guo, Non-invasive monitoring of in vivo hydrogel degradation and cartilage regeneration by multiparametric MR imaging, Theranostics 8 (4) (2018) 1146–1158, https://doi.org/10.7150/thno.22514.
[38] X. Nie, Y.J. Chuah, W. Zhu, P. He, Y. Peck, D.A. Wang, Decellularized tissue engineered hyaline cartilage graft for articular cartilage repair, Biomaterials 235 (2020) 119821, , https://doi.org/10.1016/j.biomaterials.2020.119821.
[39] T. Guo, M. Noshin, H.B. Baker, E. Taskoy, S.J. Meredith, Q. Tang, J.P. Ringel, M.J. Lerman, Y. Chen, J.D. Packer, J.P. Fisher, 3D printed biofunctionalized scaffolds for microfracture repair of cartilage defects, Biomaterials 185 (2018) 219–231, https://doi.org/10.1016/j.biomaterials.2018.09.022.
[40] H. Chen, J. Qin, Y. Hu, Efficient Degradation of High-molecular-weight hyaluronic acid by a combination of ultrasound, hydrogen peroxide, and copper ion, Molecules 24 (3) (2019) 617, https://doi.org/10.3390/molecules24030617.
[41] K.J. Wolf, S. Kumar, Hyaluronic acid: incorporating the bio into the material, ACS Biomater. Sci. Eng. 5 (8) (2019) 3753–3765, https://doi.org/10.1021/acsbiomaterials.8b01268.
[42] M. Boesen, K.E. Jensen, E. Qvistgaard, B. Danneskiold-Samsoe, C. Thomsen, M. Ostergaard, H. Bliddal, Delayed gadolinium-enhanced magnetic resonance imaging (dGEMRIC) of hip joint cartilage: better cartilage delineation after intra-articular than intravenous gadolinium injection, Acta Radiol. 47 (4) (2006) 391–396, https://doi.org/10.1080/02841850600596792.
[43] D. Burstein, J. Velyvis, K.T. Scott, K.W. Stock, Y.-J. Kim, D. Jaramillo, R.D. Boutin, M.L. Gray, Protocol issues for delayed Gd(DTPA)$^{2-}$-enhanced MRI (dGEMRIC) for clinical evaluation of articular cartilage, Magn. Reson. Med. 45 (1) (2001) 36–41, https://doi.org/10.1002/1522-2594(200101)45:1<36::aid-mrm1006>3.0.co;2-w.
[44] W. Wong, K.W. Chan, Gadolinium complexes as MRI contrast agents for diagnosis, in: C. Huang (Ed.), Rare Earth Coordination Chemistry: Fundamentals and Applications, John Wiley & Sons (Asia) Pte Ltd., Singapore, 2010, pp. 407–433.
[45] S.T. Wang, Z.X. Hua, D.X. Fan, X. Zhang, K. Ren, Gadolinium retention and clearance in the diabetic brain after administrations of gadodiamide, gadopentetate dimeglumine, and gadoterate meglumine in a rat model, BioMed Res. Int. 2019 (2019) 1–12, https://doi.org/10.3978/j.issn.2223-4292.2011.08.03.